

## GEOCHEMICAL AND RADIOACTIVITY CHARACTERIZATION OF ROCKS FROM THE RIO PRETO (GO) PROJECT

Cynthia Romariz Duarte<sup>1</sup>, Daniel Marcos Bonotto<sup>2</sup> and Marcos Aurélio Farias de Oliveira<sup>2</sup>

Recebido em 22 março, 2011 / Aceito em 27 junho, 2012  
Received on March 22, 2011 / Accepted on June 27, 2012

**ABSTRACT.** The Rio Preto Project, developed by the extinct Brazilian nuclear state company, Nuclebrás, during the late 70s and early 80s, consisted of basic geological mapping and radiometric characterization by aerogeophysical gamma-ray spectrometry, without channel discrimination, of a surface area of 650 km<sup>2</sup> located to the west of the Chapada dos Veadeiros National Park on the northeastern of Goiás State, Brazil, including the confluence area of Claro and Preto Rivers. Additionally, the natural radioelements U, Th and <sup>40</sup>K were determined by gamma-ray spectrometry in 300 rock samples from cores of the Rio Preto Project area. The tests were conducted at LABIDRO-Isotopes and Hydrochemistry Laboratory of the Department of Petrology and Metalogeny (DPM) of the Institute of Geosciences and Exact Sciences, UNESP, in Rio Claro, SP, Brazil. This paper reports the results of petrographic characterization and chemical analyses of major oxides (SiO<sub>2</sub>, TiO<sub>2</sub>, Al<sub>2</sub>O<sub>3</sub>, Fe<sub>2</sub>O<sub>3</sub>, MgO, MnO, K<sub>2</sub>O, Na<sub>2</sub>O, CaO and P<sub>2</sub>O<sub>5</sub>) for all samples used to determine the natural radioelements present in the region. The organic matter content results obtained by colorimetry are also reported for selected cores of different lithotypes in order to investigate the possible relationship between graphite and the radioelements uranium and thorium. Finally, uranium content and <sup>234</sup>U/<sup>238</sup>U activity ratio data for selected samples of schists and gneisses of the Lower Member of the Ticunzal Formation suggest the influence of weathering processes in the area.

**Keywords:** Rio Preto (GO) Project, natural radioelements, gamma and alpha spectrometry.

**RESUMO.** A extinta Nuclebrás, no final da década de 70 e início dos anos 80, conduziu o Projeto Rio Preto, por intermédio do qual efetuou o mapeamento geológico básico e a caracterização radiométrica por aerogamaespectrometria, sem discriminação de canais, da região nordeste do estado de Goiás, Brasil, a oeste da área do Parque Nacional da Chapada dos Veadeiros, perfazendo um total de 650 km<sup>2</sup> e englobando a confluência dos rios Claro e Preto. Os radioelementos naturais U, Th e <sup>40</sup>K do Projeto Rio Preto (GO) foram posteriormente caracterizados por espectrometria gama aplicada aproximadamente a 300 amostras, a qual foi conduzida no LABIDRO-Laboratório de Isótopos e Hidroquímica do Departamento de Petrologia e Metalogenia (DPM) do Instituto de Geociências e Ciências Exatas da UNESP-Campus de Rio Claro, SP, Brasil. Este trabalho descreve para todas as amostras os resultados obtidos na caracterização petrográfica e análise química dos principais óxidos (SiO<sub>2</sub>, TiO<sub>2</sub>, Al<sub>2</sub>O<sub>3</sub>, Fe<sub>2</sub>O<sub>3</sub>, MgO, MnO, K<sub>2</sub>O, Na<sub>2</sub>O, CaO e P<sub>2</sub>O<sub>5</sub>), os quais foram utilizados na avaliação da ocorrência dos radioelementos naturais naquela área. Também são apresentados resultados do teor de matéria orgânica obtido por colorimetria em amostras selecionadas de diferentes litotipos para melhor investigar a possibilidade de relação entre a grafita e os radioelementos urânio e tório. Finalmente, dados da concentração de urânio e razão de atividade <sup>234</sup>U/<sup>238</sup>U em amostras selecionadas de xistos e gnaiesses da Formação Ticunzal – Membro Inferior sugeriram a influência de processos intempéricos na área.

**Palavras-chave:** Projeto Rio Preto (GO), radioelementos naturais, espectrometria gama e alfa.

---

<sup>1</sup>Departamento de Geologia/Centro de Ciências/UFC Campus do Pici, Bloco 912, 60455-760 Fortaleza, CE, Brazil. Phone: +55(85) 3366-9867

– Email: cynthia.duarte@ufc.br

<sup>2</sup>Departamento de Petrologia e Metalogenia/Instituto de Geociências e Ciências Exatas (IGCE)/UNESP, Avenida 24-A, 1515, P.O. Box. 178, Bela Vista, 13506-900 Rio Claro, SP, Brazil. Phone: +55(19) 3526-9257; Fax: +55(19) 3524-9644 – E-mails: dbonotto@rc.unesp.br; maurelio@rc.unesp.br

## INTRODUCTION

In Brazil, the systematic exploration of radioactive minerals began in 1952, under the supervision of the National Research Council (later, CNPq) with the participation of Brazilian and American geologists from the United States Geological Survey (USGS) and U.S. Atomic Energy Commission, the first traces of uranium were detected in Poços de Caldas (MG), Jacobina (BA) and Araxá (MG). In 1956, when the Comissão Nacional de Energia Nuclear (CNEN) was created, a prospecting program was established together with the USGS. Later on, between 1962 and 1966, an agreement between CNEN and Commissariat à l'Énergie Atomique, CEA, created an exchange program for French and Brazilian technicians. Between 1966 and 1974, the exploration of uranium was under the responsibility of CNEN, and from the 70s, the Companhia de Pesquisa de Recursos Minerais, CPRM, shared this responsibility. In 1974, when Empresas Nucleares Brasileiras S.A., NUCLEBRÁS, was created, Brazil also had a nuclear program that consisted of prospection, researching, mining and industrialization of uranium minerals (Javaroni & Maciel, 1985).

In 1988, INB succeeded Nuclebrás and, in 1994 they became one company when it incorporated its subsidiaries Nuclebrás Enriquecimento Isotópico S.A. (Nuclei); Urânio do Brasil S.A. and Nuclemon Mínero-Química Ltda, activities and assignments as well. The programs for uranium prospection and research identified nine major uranium deposits in Brazil, totaling 301,490 tons of  $U_3O_8$ . The major uranium deposits in Brazil are: Itataia (CE); Espinharas (PB); Lagoa Real (BA); Campos Belos/Rio Preto and Amorinópolis (GO); Quadrilátero Ferrífero and Poços de Caldas (MG); Figueira (PR) (Javaroni & Maciel, 1985) and Pitinga (AM) (Majdalani, 1999).

The Rio Preto Project conducted by Nuclebrás during the late 70s and early 80s consisted of basic geological mapping and radiometric characterization by aerogamma-spectrometry of a 650-km<sup>2</sup> area west of the Chapada dos Veadeiros National Park on the northeastern of Goiás State that included the confluence of Rio Claro and Rio Preto, the latter a tributary of Rio Tocantins. From the measured and inferred uranium reserves in Brazil, the largest and smallest are, respectively, Itataia (CE) (142,500 tons of  $U_3O_8$ ) and Rio Preto (GO) (1,000 tons of  $U_3O_8$ ) (Javaroni & Maciel, 1985).

The growing interest in recent years in the use of uranium as nuclear fuel, associated to its rising price in the international market, has motivated basic research in occurrence areas, even the ones with small reserves like Rio Preto, in Goiás. Duarte &

Bonotto (2000, 2006) conducted laboratory radiometric characterization by gamma-ray spectrometry with channel discrimination in samples from the geological mapping performed by Nuclebrás in the late 70s and early 80s, as well as in samples collected in early 2001, when field work was conducted in the area in order to densify the grid points.

This study shows the results of petrographic characterization of the main lithological types found in the Rio Preto (GO) project area and geochemical analysis of the major oxides ( $SiO_2$ ,  $TiO_2$ ,  $Al_2O_3$ ,  $Fe_2O_3$ ,  $MnO$ ,  $MgO$ ,  $CaO$ ,  $Na_2O$ ,  $K_2O$  and  $P_2O_5$ ), which allowed us to elaborate diagrams of parameter variations and to separate the lithotypes according to their mineralogical and chemical composition. Last, this information was combined with radiometric data in order to better understand the aspects related to natural radioelement occurrence (U, Th and  $^{40}K$ ) in the investigated area.

## OVERVIEW OF THE STUDY SITE

The 650-km<sup>2</sup> study site is located on the northwest of Goiás State (Fig. 1), between 47°50' and 48°05'W latitudes and 13°47' and 14°00'S longitudes, and includes the confluences of Rio Claro and Rio Preto. It is located west of the Chapada dos Veadeiros National Park, a region with extensive plateaus and many rivers, including a large number of waterfalls and lakes with crystal clear water excellent for swimming.

The drainage of the larger area is part of the Tocantins River Basin, from which Rio Preto is a tributary; while the study site is drained by the Rio Preto and its tributaries, of which the Rio Claro is the most important. These two rivers cover a wide and dense drainage network, which reflects the underlying structure and lithology. In gneissic substrates, drainage has an open dendritic pattern with low branch density; while in schists, the dendritic pattern is denser, with valleys in closed "V". Upon the occurrence of dome structures, such as granite and granodioritic gneiss bodies, the drainage pattern is radially divergent (Figueiredo Filho et al., 1982). There is a strong structural control on the relief and drainage, with very striking EW and secondary NW relief alignments. The drainage has three principal alignment directions, indicating the EW, NS and NW existing fractures.

The research area is located in the Plateau Region of Central Goiás State, more specifically in the Complexo Montanhoso Veadeiros, Araí (Lacerda Filho et al., 2000). This region is part of the Planaltos de Estruturas Dobradas (Folded Structures Plateaus) domain and reproduces relief features resulting from the exhumation of folded structures over several tectonic cycles, reflected through different structural styles that explain its particularities.

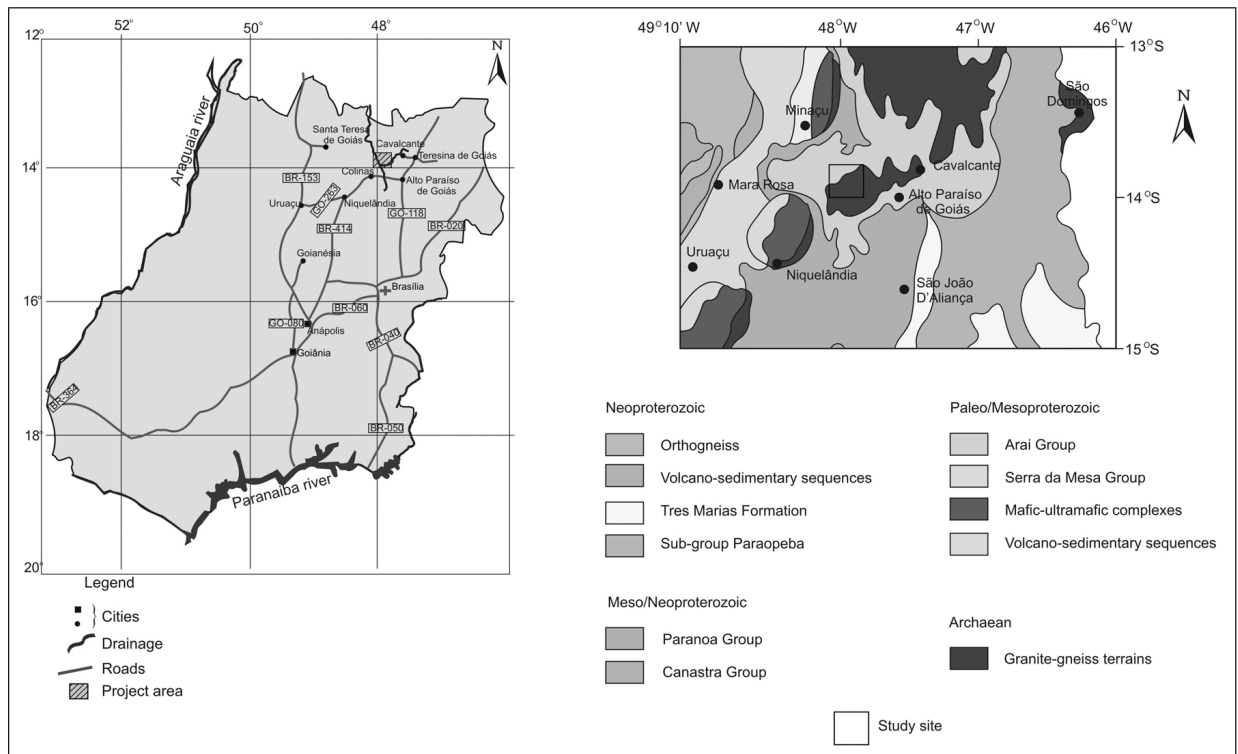


**Figure 1** – Map of the study site located in the State of Goiás, Brazil, and lithostratigraphic column of the Pale-Meso-Neoproterozoic units in the Brasília Belt, according to Dardenne (2000).

According to Ross (1985) these plateaus and mountains are associated with the Brasília Folded Belt and extend from northern Goiás State to the southwest of Minas Gerais State, often supported by metamorphic rocks, mainly quartzite, associated in some places with granite intrusions. The large flat tops like mesas occur frequently in the region.

Campos et al. (2009) suggest that the region may be divided into three geomorphological compartments, whose evolution is closely linked to the bedrock substrate and tectonic structure. The first compartment consists of the mountains to the north, where quartzites are the predominant lithology with the highest elevations in Serra do Ticunzal. The second compartment consists of plateaus on the western portion characterized by elevated areas with more uniform relief and isolated hills that enhance the regional landscape. The third compartment is characterized by the Rio Claro and Rio Preto lowland central area, corresponding to a vast peneplained area, with an undulated morphology, developed over gneisses and schists of the Basal Complex and Ticunzal Formation, with the presence of Tertiary-Quaternary covers. The contact between the lowland and mountain compartments, to the north of the area is marked by an EW escarpment. The climate

in the region is AW Köppen type: tropical, hot, semi-humid, characterized by a dry winter season, from April to September, and a rainy summer season between October and March. The average annual rainfall is between 1500 and 1700 mm (Martins, 1999).

The soil of the region is poor and acidic due to intense leaching and laterization processes. Latosols and laterites cover large and slightly dissected terrains, occurring on its borders, gravelly regolith soils, with lateritic concretions and semi-altered rock fragments. Lateritic-saprolite also occurs in small lateritic pavements over schists and phyllites, while deeper latosols can be formed on the slopes of granite massifs. Extensive alluvial-colluvial sandy coverage occurs at the foot of the lateritic and quartzitic escarpments, which are commonly called “areíões” (Pinto, 1986).

The Chapada dos Veadeiros have typical flora and fauna of the Brazilian Cerrado. The Cerrado trees are sinuous and crooked due to the presence or absence of water and nutrients. In the higher areas yellow latosols dominate, followed by red, dark red, grey and black. The leaves are usually deciduous, falling during the dry period to prevent water loss by the plants (Chapada, 2000).

## REGIONAL AND LOCAL GEOLOGY

The studied site is located on the northern portion of the Brasília Fold Belt, Tocantis Province (Almeida et al., 1977), in Central Brazil, between the São Francisco and Tapajós Cratons, is a geotectonic entity formed by rocks of different ages, tectonically stable since the end of the Brasiliano Cycle. In Goiás, they are characterized by thick sequences of folded and supracrustal rocks metamorphosed during the Brasiliano Cycle (Brasília, Araguaia and Paraguay belts), Archaean fragments of essentially granite-gneiss composition, where greenstone belt type volcano-sedimentary sequences are included, and by ancient granulite terrains, also formed during the Brasiliano Cycle (Lacerda Filho et al., 2000).

Dardenne (2000) suggests that the Tocantins Province represents a large orogeny developed during the Neoproterozoic, resulting from the convergence and collision of three major continental blocks: NW, the Amazon Craton; E, the São Francisco Craton and a to the SW, the craton under the Parana Basin. This orogeny is formed by Paraguay-Araguaia and Brasília folding belts. The Brasília belt is formed by ancient units such as granite-greenstone terrain and granite-gneiss basement, thick sedimentary and metasedimentary sequences, igneous intrusions and volcano-sedimentary sequences of different ages (Fig. 1). The Granite-gneissic complex, Ticunzal Formation and Arai Group, among the various lithostratigraphic units present in the Brasília belt, are relevant in the study site.

The Archaean and Paleoproterozoic rocks of the basement belonging to the Granite-Gneissic Complex comprises porphyroblastic gneisses, granodioritic-tonalitic orthogneisses, granodioritic bodies and subordinate schists. Migmatitic cores, pegmatite veins and basic rock dikes are also present in this unit (Andrade et al., 1981, 1985). The rocks of the Granite-Gneissic Complex crop out along stream talwegs such as sample 193 sampled on the SW of the study site. Other outcrops occur in waterfalls, such as in Cachoeira Vêu da Noiva, in São Bentinho Stream (sample 137), as large rounded outcrops (Core 131) or metric size bodies (Core 138). The granodioritic bodies are characterized by intense cataclasis and consist of quartz, biotite, plagioclase, with opaques and zircon as main accessories. Sericite is highlighted among the products of weathering. Pegmatite occurs as veins or pockets without zoning. They are, in general, discordant structures from the host rocks and the most representative are 2 m thick.

Stratigraphically above the Granite-Gneissic Complex occurs the Ticunzal formation, a set of schists interlayered with parag-

neisses at the base (Fig. 2). The most common lithologies are generally graphitic biotite-muscovite schists and paragneisses. Other schist varieties include types with subordinate garnet, chlorite and tourmaline. The Ticunzal Formation is divided into Lower and Upper Members. The Lower Member with estimated thickness up to 300 m is a sequence of gneisses intercalated with graphite schists. The graphite schists of the Upper Member shows increasing quartz content upwards presenting quartz-schists at the top. At this stratigraphic level, quartz-schists are interspersed with garnet and tourmaline bearing schist, with little or no graphite and abundant quartz. The estimated average thickness for this unit is 250 m.

Above the Ticunzal Formation lies the Arai Group, a set of metamorphic rocks consisting of psamites at the base and mudstones at the top (Andrade et al., 1981, 1985). The metamorphism reaches the green schist facies, biotite zone. The Group was divided into two formations, Arraias (at the base) and Trairas (at the top); the first consists of quartzitic sequences responsible for the main topographic elevations of the region, while the second located to the NW, is more pelitic than Arraias Formation and consists of mica schists and metasiltstone. The depositional setting of the Arai group has been related to an intracontinental rift environment, which began at about 1,8 Ga (Lacerda Filho et al., 2000) with sediment deposition of the Arraias Formation, manifestations of acid to basic volcanism and contemporaneity of granitic intrusions.

The host rocks of the Ticunzal Formation are characteristically polytectonic and polymetamorphic, displaying all deformations that affected the Arai Group. A striking feature is the presence of relicts of muscovite crystals, deformed during the Brasiliano shearing (Lacerda Filho et al., 2000). Underlying the rocks of Arai Group to the northwest, some acidic intrusive bodies of granitic composition cut the Granite-Gneissic Complex and the Ticunzal Formation.

There are also, in the study area, detrital-lateritic covers formed by lateritic layers associated with the clay-sandy soil and alluvial deposits represented by flat surfaces with slight undulations near the interfluves of the lowest order drainages.

## MATERIALS AND METHODS

Approximately 300 samples, from outcrops located with GPS, were analyzed. All the lithotypes found in the study area were sampled, but emphasis was given to the rocks of Ticunzal Formation, where the uranium reserves are located. Petrographic characterization focusing on the Lower Member of the Ticunzal

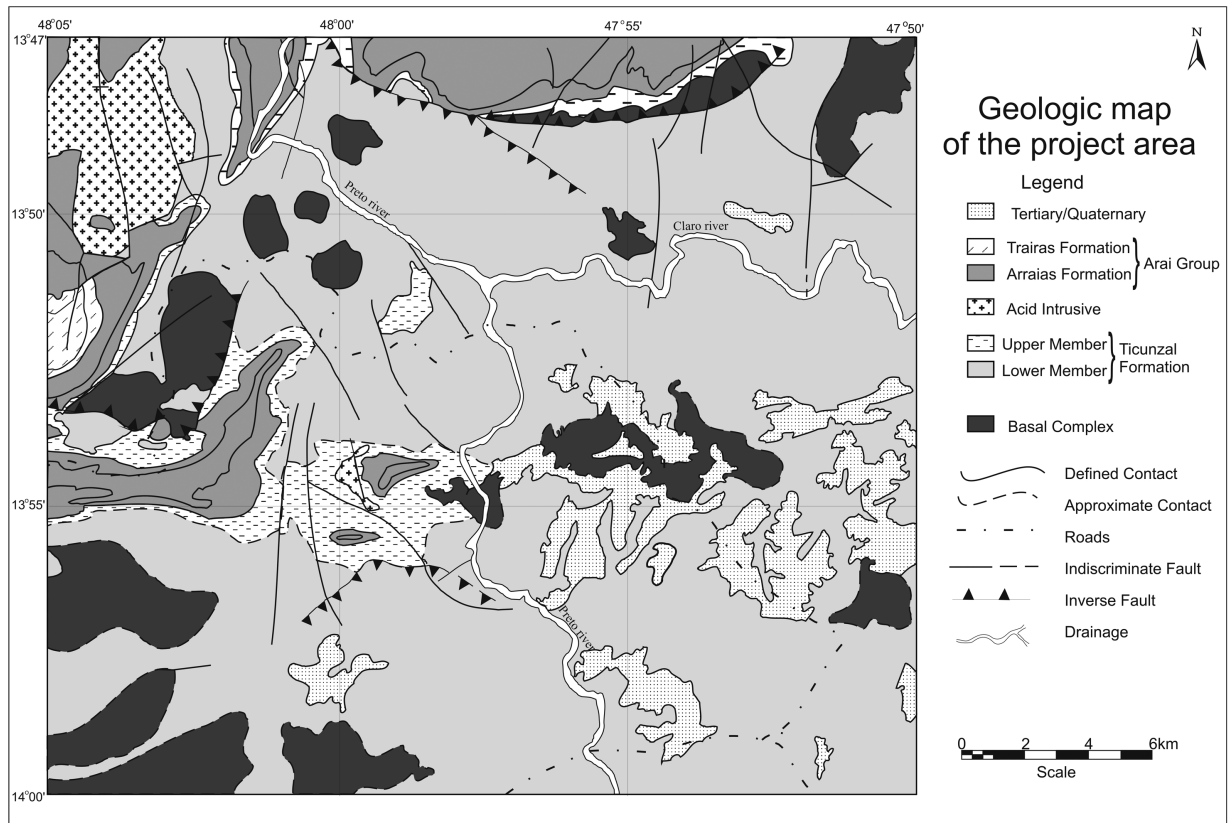


Figure 2 – Geological map of the study site according to Andrade et al. (1985).

Formation was conducted to determine lithotype mineralogy. The thin sections analyzed belong to the following lithological units: Basal Complex, Ticunzal Formation (Lower and Upper Member), basic rock dikes and Arraias Formation.

The Basal Complex consists mainly of gneisses, orthogneisses and subordinate schists. In these lithologies, potassium feldspar, quartz, plagioclase and biotite are common, while crystals of apatite, zircon and opaque are accessories. Sericite is the main alteration mineral. In some cases there is epidotization. Orthoclase may constitute some porphyroblastic crystals in the gneisses. Muscovite is also found in some thin sections of the orthogneisses. The texture of the rock types found in the Basal Complex varies from porphyroblastic to cataclastic, including the granoblastic textures of the gneisses and lepidoblastic textures of the schists, and in many cases grano-lepidoblastic alternating bands.

In the Lower Member of the Ticunzal Formation, the most common rocks are biotite-muscovite-schists and paragneisses. The paragneisses consist essentially of plagioclase, quartz, biotite and garnet, whose textures range from granoblastic to grano-

lepidoblastic. The accessory minerals are epidote and muscovite. The textural and mineralogical characterization of paragneisses indicated the presence of altered feldspar crystals, as well as recrystallized quartz and biotite, with striking alternating granoblastic and lepidoblastic bands. Another textural aspect of predominantly granoblastic paragneisses consists of garnet crystals clusters, surrounded by very fine muscovite crystals.

The schists from the Lower Member of the Ticunzal Formation consist mainly of quartz and muscovite; with common accessories biotite, garnet, kyanite and opaques. The striking textural aspect of these schists is the alternation between lepidoblastic and granoblastic beds. The schists may still have tourmaline levels between the quartz and micaceous levels. Tourmaline can occur more abundantly, forming tourmalinites, due to active hydrothermal processes. There is also disseminated graphite that locally forms entirely graphitic levels between the quartz and micaceous levels.

The lithology of the Upper Member of the Ticunzal Formation is predominantly represented by schists consisting of muscovite, quartz, biotite and disseminated graphite, with the presence of

tourmalines in some cases and garnet in others, while sericite and rutile occur as accessories. The texture is characterized by alternating lepidoblastic levels, defined by bi-directional orientation of the micaceous minerals and granoblastic levels of quartz. The brown color commonly observed in the schists of Upper and Lower Members of the Ticunzal Formation is due to the oxidation of iron-containing minerals, such as biotite.

In the northern part of the area, there are basic dikes, represented by diabase, consisting mainly of pyroxene, plagioclase and opaques with discrete occurrence in the middle of the Ticunzal Formation. The Arraias Formation lithology varies widely. The sampled levels are characterized by micaceous quartzite and quartz-muscovite-schists, with expressive alternation between the granoblastic and lepidoblastic levels.

After petrographic analysis, the samples were cut, crushed and pulverized at the Department of Petrology and Metallogeny (DPM) of the State University of São Paulo (UNESP, in Rio Claro). A small amount of the pulverized sample was sent to LABOGEO, of UNESP, in Rio Claro, in order to perform the chemical analysis by X-ray fluorescence (Gomes, 1984). Table 1 shows oxide percentages, and sample lithotype of each sampling station. Loss on Ignition (LOI) data are also displayed in Table 1, which expresses the sum of organic matter, adsorbed and crystal lattice water, fluid inclusions, CO<sub>2</sub> from carbonates and SO<sub>2</sub> from sulfides (Faure, 1991) in the samples.

Although LOI is related to the organic matter (OM), OM additional analysis of selected samples of varied lithotypes was performed by colorimetry (Hach, 1992), in order to investigate in detail the relationship between graphite (carbon) and the radioelements uranium and thorium, according to Duarte & Bonotto (2006). Organic matter has been recognized as an important binding of these radioelements (Langmuir, 1978).

The use of alpha spectrometry to analyze rocks, minerals and waters has been widely described in the literature, as reviewed by Ivanovich & Harmon (1992). In this work, the methodology established by Bonotto (2004) was used to determine uranium concentration and <sup>234</sup>U/<sup>238</sup>U activity ratio of selected cores of schists and gneisses from the Lower Member of the Ticunzal Formation. For some schist samples, the removal of the altered portion was not possible since the entire rock was altered.

## DISCUSSION

### TiO<sub>2</sub>-SiO<sub>2</sub> diagrams

Silica predominance in the samples is evident and expected for the lithotypes found in the area. Samples 8B and 36A are lateritic-ferruginous concretions, presenting low SiO<sub>2</sub> content (18 and

24%, respectively. SiO<sub>2</sub> contents over 75% were found in samples 7, 16, 20, 23, 27, 36B, 39, 54, 63, 72, 75, 82, 83, 121, 122, 127, 136, 140, 143, 176 and 187, while values above 98% occur in sandstones and quartzites.

Since the stratigraphic units are heterogeneous and display very significant lithological variation, the lithotypes were separated in groups of gneisses, fresh and altered schists of the Ticunzal Formation Lower Member, schists of the Ticunzal Formation Upper Member, as well as gneisses and gneissic granites of the Basal Complex. The other lithotypes, such as tourmalinites, quartzites, sandstones and pegmatites were not used in the classification because they are discontinuous occurrences, forming lenses, veins and pockets.

The data obtained for each group were represented in the TiO<sub>2</sub> vs. SiO<sub>2</sub> diagram of Tarney (1976), which allowed us to evaluate the igneous and sedimentary character of the analyzed samples. The diagram obtained for the gneisses and gneissic granites of the Basal Complex shows a mixture of para- and ortho-derived rocks in the samples (Fig. 3a). The diagrams for the gneisses of the Ticunzal Formation Lower Member show several igneous rocks samples, whereas a greater number of para-derived rocks was expected (Fig. 3b).

The Lower Member of the Ticunzal Formation also presents intercalations of micaceous schists, graphitic or not, locally with tourmaline and garnet. They were separated into two groups, consisting mainly of muscovite and biotite schists, the latter more often altered. The fresher schists form a group where the ortho- and para-derived rocks are mixed, according to the classification proposed by Tarney (1976) (Fig. 3c), while the altered biotite schists have a more homogeneous behavior, and are almost exclusively classified as para-derived rocks, as seen in Figure 3d.

The schists of the Upper Member of the Ticunzal formation are also essentially metasedimentary, according to the classification used (Fig. 3e), which was expected for this unit. The remaining stratigraphic units were not classified due to their great lithological variability.

### Correlation statistical analysis

Correlation statistical tests were performed for all oxides present in the main lithotypes of the Ticunzal Formation. The rocks of the Lower Member were divided into three lithological groups, that is, gneisses (n = 93), fresh schists (n = 26) and altered schists (n = 63). The other rocks from the Lower Member correspond to interbedded quartzite, sandstone lenses, pegmatite veins, among others and were not included in the correlation analysis.

**Table 1** – Results of chemical analysis (%) for the samples from the study area. LOI = loss on ignition.

Core	Lithotype	SiO <sub>2</sub>	TiO <sub>2</sub>	Al <sub>2</sub> O <sub>3</sub>	Fe <sub>2</sub> O <sub>3</sub>	MnO	MgO	CaO	Na <sub>2</sub> O	K <sub>2</sub> O	P <sub>2</sub> O <sub>5</sub>	LOI
Tertiary/Quaternary												
82	Sandstone	93.53	0.04	3.66	1.48	0.01	0.07	0.02	0.02	0.20	0.36	0.60
83	very altered Sandstone	96.90	0.01	1.09	0.86	0.02	0.06	0.05	0.22	0.22	0.37	0.18
Arai group												
95	Graphite schist	40.22	0.96	29.10	10.31	0.14	1.37	0.013	0.32	6.68	0.10	10.77
96	Yellow Schist	47.97	1.15	26.43	9.69	0.03	1.61	0.014	0.13	6.68	0.07	6.29
97	Rose Migmatitic Gneiss	65.11	0.09	22.24	0.78	0.02	0.07	0.193	3.14	5.46	0.01	2.75
98	Graphite schist	57.03	0.67	24.95	5.19	0.02	0.71	0.010	0.25	5.64	0.04	5.48
140	Quartzite	81.14	0.25	12.55	1.03	0.01	0.11	0.023	0.24	3.89	0.06	0.69
141	Crenulated Sericite quartz schist	53.09	0.67	28.10	5.89	0.05	1.19	0.025	0.30	6.44	0.42	4.20
187	Quartzite fractured	78.32	0.23	14.51	1.09	0.01	0.29	0.020	0.21	4.32	0.05	0.95
217	Fresh Muscovite schist	51.77	0.71	30.70	2.76	0.01	0.81	0.021	0.26	11.24	0.08	1.65
218	Muscovite schist	51.78	0.21	30.19	2.69	0.01	0.97	0.007	0.31	10.10	0.03	3.68
257	Very altered Schist	49.98	0.47	31.66	7.20	0.01	1.12	0.03	0.25	7.93	0.07	1.28
258	Very altered Schist	50.59	0.24	31.79	7.64	0.01	0.88	0.03	0.50	6.92	0.04	1.37
Intrusive Acid												
150	Biotite granite	56.15	0.74	26.92	7.71	0.03	1.24	0.01	0.40	6.27	0.11	0.41
206	Biotite granite	66.87	0.58	15.47	5.52	0.11	0.35	1.31	2.69	5.67	0.56	0.85
207	Banded Biotite granite	65.49	0.29	19.30	2.04	0.04	0.99	0.69	3.94	5.39	0.24	1.59
Formation Ticunzal – Upper Member												
93	Quartz muscovite schist	65.16	1.03	19.23	3.52	0.02	1.83	0.03	0.10	6.57	0.12	2.38
94	Muscovite schist	46.51	0.88	24.89	8.61	0.07	1.12	0.02	0.31	5.57	0.11	11.90
99	Granada muscovite schist	50.48	0.86	29.49	6.49	0.08	1.38	0.16	0.82	6.99	0.04	3.21
100A	Gneiss	52.13	0.57	30.47	4.37	0.05	1.14	1.10	1.77	2.71	0.10	5.59
100B	Schist	42.52	0.54	38.25	5.32	0.04	0.68	0.65	0.93	2.21	0.16	8.67
101	Graphite schist	61.24	0.70	19.33	7.33	0.01	1.10	0.15	0.28	4.25	0.03	5.59
102	Biotite muscovite schist	46.36	1.09	29.56	7.91	0.03	1.19	0.005	0.13	8.65	0.11	4.97
103	Altered red Schist	46.89	1.02	30.61	8.44	0.01	0.39	0.01	0.40	7.53	0.17	4.54
149	Biotite schist very altered	48.05	1.02	29.31	13.64	0.20	0.75	0.02	0.34	5.70	0.11	0.86
151	Gneiss	62.15	0.79	18.10	7.26	0.05	3.37	0.06	0.21	5.56	0.03	2.40
152	Graphite schist	52.85	0.96	21.11	13.77	0.08	0.50	0.01	0.21	4.91	0.05	2.54
153	Altered Gneiss	63.02	0.92	22.24	9.03	0.03	0.11	0.005	0.45	3.70	0.11	0.38
154A	Altered Biotite schist	46.83	1.24	29.65	11.21	0.03	1.85	0.01	0.28	8.27	0.16	0.47
154B	Altered Schist	49.69	0.92	29.11	9.68	0.05	2.09	0.02	0.31	7.77	0.06	0.31
155	Altered Schist	51.15	0.96	24.74	8.85	0.05	2.50	0.01	0.12	8.17	0.10	3.36
156	Altered biotite schist	50.00	0.93	25.93	10.95	0.03	2.08	0.01	0.06	8.34	0.12	1.55
157	Quartz schist	66.93	0.70	18.74	4.57	0.02	2.25	0.02	0.16	5.44	0.04	1.14
158	Orange altered Schist	54.73	0.93	26.81	6.50	0.02	0.84	0.004	0.25	8.09	0.23	1.60
159	Pegmatite pocket with quartz and tourmalines amidst schist	64.51	0.15	24.35	1.11	0.01	0.33	0.01	0.42	6.65	0.04	2.41
160	Quartz altered schist	67.49	0.34	17.22	2.63	0.04	1.03	2.72	5.07	1.80	0.10	1.56
203	Muscovite schist	50.84	0.85	28.87	3.72	0.01	1.57	0.02	0.47	9.20	0.15	4.30
204	Biotite gneiss fine	62.11	0.42	20.93	2.71	0.04	0.94	0.84	2.95	6.80	0.55	1.71
234	Gneiss fine	59.26	0.49	22.52	5.11	0.03	2.07	1.22	2.57	3.77	0.31	2.65

Table 1 – (continuation)

Core	Lithotype	SiO <sub>2</sub>	TiO <sub>2</sub>	Al <sub>2</sub> O <sub>3</sub>	Fe <sub>2</sub> O <sub>3</sub>	MnO	MgO	CaO	Na <sub>2</sub> O	K <sub>2</sub> O	P <sub>2</sub> O <sub>5</sub>	LOI
240	Fresh biotite schist	41.23	2.69	24.65	14.91	0.07	4.44	0.03	0.12	9.07	0.26	2.52
268	Muscovite biotite schist	53.98	0.74	23.68	11.08	0.06	3.33	0.08	1.54	2.65	0.12	2.74
269	Very altered Schist	51.12	0.43	29.82	10.86	0.01	0.40	0.02	0.89	5.43	0.02	1.02
Dike of basic rock												
241	Dibase	49.06	2.03	13.64	14.33	0.19	6.03	9.61	3.08	0.37	1.04	0.61
Ticunzal Formation – Lower Member												
01	Biotite gneiss	68.20	0.21	18.83	1.48	0.02	0.53	0.50	3.65	5.42	0.17	0.97
02	Altered red Schist	44.67	0.82	25.60	14.57	0.01	1.31	0.02	0.05	6.57	0.18	6.19
03	Altered red Schist	52.77	0.69	24.89	9.87	0.02	1.47	0.01	0.14	6.58	0.07	3.49
04	Leucocratic Gneiss	69.01	0.18	17.88	1.43	0.02	0.31	0.68	2.83	6.25	0.57	0.84
05	Gneiss in blocks	68.58	0.24	17.79	1.75	0.05	0.31	0.70	3.50	5.88	0.38	0.80
07	Sandstone	98.63	0.01	0.70	0.41	0.03	0.09	0.01	0.002	0.07	0.01	0.06
08A	Reddish Schist	46.57	1.24	28.06	9.46	0.02	1.45	0.01	0.09	7.23	0.09	5.77
08B	Lateritic Canga	18.10	0.29	10.77	58.70	0.01	0.12	0.01	0.01	0.72	0.05	11.22
09	Leucocratic Gneiss	67.37	0.22	20.21	1.53	0.01	0.33	0.42	2.87	5.47	0.14	1.41
10	Altered Schist with quartz vein	56.64	0.96	24.36	5.88	0.02	1.60	0.02	0.10	7.37	0.11	2.94
11	Altered Schist	47.02	1.17	26.88	8.98	0.03	2.34	0.01	0.07	8.15	0.04	5.31
12	Sandy schist	49.21	0.74	26.52	12.44	0.05	0.72	0.01	0.24	5.82	0.13	4.12
13	Altered Schist (large blocks)	47.25	1.07	29.93	8.51	0.02	0.60	0.02	0.22	6.56	0.11	5.70
14	Leucocratic Gneiss	67.55	0.29	18.60	2.27	0.02	0.47	0.33	3.88	5.77	0.16	0.66
15	Altered Schist, with quartz veins	46.78	1.26	28.44	12.87	0.03	0.66	0.01	0.13	5.23	0.08	4.50
16	Sandstone with quartz veins	93.10	0.01	0.70	0.27	0.02	0.005	0.03	0.05	0.06	0.01	5.76
17	Green Muscovite schist	46.98	0.01	36.48	1.11	0.02	0.20	0.01	0.24	11.09	0.04	3.83
18	Altered red Schist	53.77	0.92	27.21	10.78	0.03	0.40	0.01	0.17	6.44	0.14	0.13
19	Altered red Schist	42.43	1.10	31.96	9.18	0.03	0.73	0.02	0.19	8.62	0.07	5.65
20	Sandstone	92.47	0.01	1.09	1.61	0.01	0.06	0.03	0.04	0.07	0.02	4.59
21	Schist, with quartz veins	47.49	1.52	29.20	11.17	0.04	1.81	0.01	0.07	8.63	0.10	0.04
23	Sandstone	97.91	0.01	1.31	0.36	0.02	0.04	0.03	0.06	0.18	0.01	0.06
24	Mica schist	71.40	0.92	15.89	2.58	0.05	0.71	0.03	0.14	4.24	0.07	3.97
25	Altered Schist	41.65	1.25	30.10	11.35	0.05	1.28	0.01	0.05	8.00	0.08	6.18
26A	Tourmalinite with muscovite	44.09	0.82	33.25	11.60	0.08	3.29	0.38	1.24	2.25	0.07	2.93
26B	Altered Schist	38.37	1.32	30.34	14.99	0.32	0.67	0.05	0.13	5.71	0.23	7.88
27	Sandstone	97.13	0.02	1.482	0.36	0.01	0.003	0.01	0.02	0.33	0.02	0.61
28	Tourmalinite	47.72	0.97	29.86	13.27	0.07	3.89	0.46	1.31	0.10	0.04	2.31
29	Muscovite schist	46.26	1.02	33.41	4.02	0.02	0.60	0.03	0.55	9.21	0.18	4.71
30A	Tourmaline schist	55.34	1.33	22.49	7.79	0.08	1.91	0.28	0.92	6.93	0.35	2.58
30B	Biotite gneiss	61.70	1.00	20.00	5.67	0.06	1.51	0.32	2.37	5.49	0.14	1.79
31	Leucocratic gneiss	63.04	0.10	22.97	1.01	0.02	0.15	0.47	6.33	3.47	0.67	1.77
32	Altered red Schist	45.67	1.04	29.71	11.54	0.03	0.97	0.02	0.08	4.61	0.12	6.21
33	Altered Schist, with quartz veins	44.11	1.30	30.16	12.30	0.02	0.34	0.01	0.21	6.31	0.13	5.10
34	Migmatitic Gneiss	70.39	0.23	18.21	1.41	0.01	0.20	0.83	6.06	1.51	0.18	0.96
35	Migmatitic Gneiss	69.46	0.08	19.39	1.10	0.01	0.09	0.39	5.16	3.25	0.09	0.96
36A	Lateritic Canga	24.22	0.67	18.08	49.22	0.01	0.20	0.01	0.11	2.24	0.08	5.17
36B	Sandstone	95.64	0.03	1.65	1.70	0.03	0.03	0.06	0.09	0.17	0.02	0.57
37	Altered Biotite schist	47.12	1.20	29.30	10.91	0.05	0.29	0.01	0.26	5.44	0.12	5.29



Table 1 – (continuation)

Core	Lithotype	SiO <sub>2</sub>	TiO <sub>2</sub>	Al <sub>2</sub> O <sub>3</sub>	Fe <sub>2</sub> O <sub>3</sub>	MnO	MgO	CaO	Na <sub>2</sub> O	K <sub>2</sub> O	P <sub>2</sub> O <sub>5</sub>	LOI
38	Migmatitic Gneiss	58.86	0.80	20.78	7.44	0.11	2.60	1.18	1.55	5.11	0.11	1.46
39	Sandstone	95.62	0.03	2.84	0.45	0.02	0.05	0.04	0.07	0.67	0.02	0.17
40	Altered Schist	45.98	1.65	28.17	14.45	0.02	0.73	0.01	0.05	7.24	0.19	1.50
41	Leucocratic gneiss	68.11	0.16	19.90	1.33	0.02	0.13	0.49	3.96	4.53	0.25	1.11
42	Leucocratic gneiss	67.35	0.22	19.15	1.71	0.02	0.28	0.32	3.29	6.38	0.18	1.11
43	Sandstone	96.34	0.02	2.40	0.35	0.03	0.100	0.07	0.15	0.41	0.02	0.10
44	Gneiss	65.38	0.24	21.30	1.31	0.02	0.32	0.26	2.47	6.87	0.34	1.48
45	Gneiss	62.90	0.25	23.06	1.52	0.02	0.31	0.24	2.52	6.96	0.20	2.03
46	Gneiss	63.85	0.15	22.44	1.46	0.02	1.08	0.31	1.50	7.04	0.34	1.83
47	Migmatitic Gneiss	67.89	0.19	18.95	1.86	0.05	0.43	0.68	2.89	5.85	0.24	0.96
48	Gneiss	65.32	0.30	19.85	1.72	0.03	0.48	0.24	1.99	8.23	0.26	1.58
49	Gneiss Migmatitic	68.48	0.12	19.33	0.93	0.01	0.14	0.58	4.22	4.97	0.29	0.93
50	Gneiss Migmatitic	67.30	0.16	18.09	1.46	0.02	0.18	0.60	3.64	5.16	2.44	0.94
51	Pegmatite with large crystals of quartz and muscovite	68.52	0.01	17.56	1.39	0.02	0.12	0.38	2.71	3.57	4.44	1.28
52	Gneiss	65.00	0.15	19.85	1.31	0.02	0.18	0.22	3.07	5.15	3.31	1.74
53	Altered Gneiss	63.64	0.22	19.40	1.59	0.02	0.25	0.41	2.99	5.78	4.46	1.22
54	Sandstone	98.24	0.04	0.49	0.77	0.01	0.10	0.02	0.03	0.04	0.21	0.06
55A	Altered Muscovite schist	44.89	1.12	26.91	11.84	0.02	0.63	0.01	0.11	6.91	2.33	5.22
55B	Sand with heavy sediments	60.23	21.37	2.31	14.97	0.45	0.01	0.03	0.00	0.24	0.31	0.07
56	Muscovite biotite schist altered	45.61	0.93	28.21	9.32	0.03	1.33	0.005	0.05	8.49	1.22	4.81
57	Folded Muscovite quartz schist	71.64	0.14	20.17	0.77	0.003	0.26	0.005	0.23	5.37	0.27	1.14
58A	Folded Muscovite quartz schist	61.11	0.20	25.30	1.55	0.004	0.48	0.004	0.02	8.49	0.52	2.31
58B	Quartz schist	63.02	0.25	23.61	2.03	0.01	0.51	0.01	0.10	7.96	0.37	2.11
59	Very fine grey Gneiss	64.50	0.26	18.82	1.52	0.02	0.22	0.43	2.87	6.16	4.11	1.09
60	Fine grey Gneiss	63.49	0.38	17.84	2.03	0.02	0.45	0.49	2.74	6.44	5.10	1.02
61	Schist	49.75	0.38	27.93	3.09	0.04	3.01	0.13	0.08	9.42	2.08	4.10
62	Altered Schist	42.02	1.48	24.39	14.67	0.06	1.87	0.03	0.10	6.87	2.30	6.21
63	Sandstone	96.67	0.01	2.00	0.41	0.02	0.02	0.03	0.06	0.39	0.31	0.07
64	Altered Schist	53.21	0.73	26.84	6.35	0.03	1.11	0.03	0.23	7.30	0.70	3.48
65	Gneiss	60.03	0.15	24.53	2.40	0.02	0.79	0.02	0.10	8.74	1.32	1.86
66	Fine Gneiss	64.99	0.04	19.70	0.84	0.02	0.04	0.30	3.56	4.57	3.89	2.04
67	Coarse Gneiss	66.78	0.14	16.98	1.47	0.03	0.41	0.50	3.60	5.11	2.16	2.82
68	Altered Schist	48.51	1.09	26.85	10.00	0.02	1.21	0.02	0.12	8.01	1.72	2.45
69A	Coarse Gneiss	67.29	0.13	17.03	1.23	0.02	0.21	0.59	3.33	5.31	2.18	2.72
69B	Gneiss finer than 69A	65.69	0.19	17.48	1.74	0.02	0.26	0.57	3.29	4.83	4.39	1.53
70	Biotite gneiss	61.20	0.44	18.98	2.08	0.02	0.59	0.45	2.22	6.64	5.62	1.76
71A	Light grey Gneiss	66.29	0.32	17.64	2.16	0.04	0.95	1.99	5.05	1.97	1.84	1.76
71B	Tourmalinite	41.63	1.18	32.32	14.05	0.15	2.98	0.65	0.93	3.71	1.38	1.02
71C	Altered Schist	49.19	0.88	25.89	8.46	0.07	2.05	0.07	0.20	7.14	1.21	4.83
71D	Biotite gneiss	67.35	0.36	17.49	2.41	0.05	1.07	2.03	4.75	2.24	1.68	0.54
72	Sandstone	97.88	0.01	0.94	0.55	0.01	0.06	0.02	0.004	0.16	0.14	0.23
73	Altered red Schist	41.33	0.87	30.70	12.79	0.02	0.52	0.01	0.23	6.22	0.67	6.64
74	Altered Schist	48.94	0.80	26.61	9.98	0.02	1.56	0.01	0.16	7.03	0.66	4.22
75	Sandstone	96.36	0.02	2.12	0.45	0.02	0.01	0.04	0.15	0.38	0.21	0.25

Table 1 – (continuation)

Core	Lithotype	SiO <sub>2</sub>	TiO <sub>2</sub>	Al <sub>2</sub> O <sub>3</sub>	Fe <sub>2</sub> O <sub>3</sub>	MnO	MgO	CaO	Na <sub>2</sub> O	K <sub>2</sub> O	P <sub>2</sub> O <sub>5</sub>	LOI
76	Gneiss	62.84	0.27	21.60	2.23	0.02	0.35	0.26	2.28	5.62	2.01	2.52
77	Gneiss	67.02	0.21	19.23	1.32	0.02	0.25	0.55	2.91	5.12	1.87	1.50
78A	Altered Biotite gneiss	47.25	0.92	27.09	8.36	0.07	1.69	0.01	0.11	8.57	1.00	4.93
78B	Muscovite schist altered	40.14	1.26	29.27	12.66	0.03	1.13	0.01	0.10	8.03	0.74	6.64
79	Gneiss	68.24	0.12	18.77	0.88	0.02	0.38	0.57	3.83	5.16	1.16	0.86
80	Gneiss fine with coarse vein	68.50	0.27	17.20	1.27	0.02	0.44	0.72	3.90	5.12	1.77	0.79
81A	Biotite schist altered	38.39	0.74	29.35	16.02	0.26	1.69	0.01	0.27	5.39	0.74	7.17
81B	Reddish Granada biotite schist	45.98	0.67	31.43	8.95	0.05	0.34	0.01	0.44	6.12	0.77	5.25
90	Gneiss	64.66	0.41	21.06	2.31	0.02	0.55	0.21	2.73	6.14	0.23	1.68
91	Leucocratic Gneiss	68.69	0.21	19.04	1.94	0.02	0.47	0.56	3.73	3.58	0.23	1.52
92	Altered Schist	51.48	1.16	25.56	7.81	0.05	2.10	0.02	0.17	7.23	0.09	4.31
104	Muscovite schist	58.17	0.95	23.31	5.06	0.02	2.00	0.01	0.07	7.93	0.09	2.40
105	Leucocratic Gneiss	65.59	0.30	21.21	1.35	0.01	0.34	0.11	1.85	6.66	0.36	2.22
106	Graphite schist	66.81	0.52	17.86	5.16	0.05	1.41	0.02	0.16	4.68	0.34	3.00
107	Gneiss	64.72	0.14	21.98	1.26	0.01	0.22	0.30	2.86	6.23	0.23	2.05
108	Biotite gneiss	60.75	0.72	23.25	4.56	0.03	1.31	0.06	0.81	6.10	0.11	2.31
109	Gneiss	68.21	0.15	19.00	1.45	0.08	0.18	0.37	3.88	5.57	0.14	0.96
110	Biotite crenulated schist	51.27	1.10	24.78	9.30	0.03	2.19	0.02	0.21	7.08	0.19	3.83
111	Tourmaline biotite schist	54.71	0.76	25.29	6.24	0.05	1.92	0.02	0.32	6.82	0.11	3.74
112	Gneiss	66.98	0.18	20.02	1.47	0.02	0.29	0.29	3.47	5.66	0.25	1.37
113	Biotite schist	46.51	1.01	29.17	8.53	0.01	1.07	0.01	0.20	8.31	0.13	5.03
114A	Altered Biotite schist	45.01	1.18	29.17	11.60	0.05	0.51	0.01	0.16	6.57	0.13	5.61
114B	Biotite schist	56.04	0.92	24.37	6.53	0.03	1.16	0.02	0.09	7.57	0.12	3.14
115	Reddish altered Schist	49.82	0.95	24.96	9.53	0.04	2.21	0.01	0.14	7.51	0.11	4.72
116	Graphite schist	50.89	0.40	25.27	7.41	0.01	0.33	0.01	0.26	5.90	0.26	9.26
117	Gneiss	62.59	0.65	20.38	5.82	0.08	1.81	0.64	1.82	3.93	0.16	2.10
118	Schist	62.52	0.62	20.80	4.00	0.01	1.41	0.01	0.06	7.14	0.06	3.37
119	Red altered Schist	50.96	0.88	29.81	6.96	0.04	1.28	0.02	0.08	6.28	0.28	3.40
120	Fractured Granada gneiss	62.44	0.06	22.79	1.28	0.01	0.14	1.09	6.89	3.12	0.75	1.40
121	Sandstone	88.71	0.02	7.18	0.79	0.01	0.16	0.10	1.06	1.64	0.10	0.22
122	Sandstone	90.96	0.02	1.50	0.37	0.01	0.001	0.03	0.06	0.30	0.02	6.72
123	Migmatitic Gneiss	66.20	0.42	19.66	2.32	0.02	0.39	0.28	2.71	6.11	0.32	1.58
124	Fine Gneiss	66.31	0.27	20.10	1.59	0.02	0.28	0.42	3.01	6.30	0.42	1.27
125	Fine altered Gneiss	67.15	0.37	19.07	2.04	0.01	0.41	0.45	3.09	5.86	0.29	1.25
126	Altered Gneiss	66.88	0.20	20.34	1.36	0.02	0.23	0.34	3.22	5.57	0.20	1.64
127	Sandstone	97.45	0.01	1.38	0.29	0.01	0.02	0.02	0.04	0.31	0.01	0.45
128	Altered Gneiss	68.30	0.16	19.30	1.04	0.01	0.12	0.26	4.06	5.15	0.15	1.45
129	Altered Gneiss	67.74	0.13	19.58	1.52	0.02	0.18	0.50	3.22	5.29	0.23	1.57
132	Altered Biotite schist	49.65	0.64	22.87	10.62	0.07	1.56	0.02	0.12	7.04	0.17	7.22
133A	Altered Gneiss	63.55	0.12	23.83	1.89	0.01	0.76	0.09	0.29	7.30	0.17	2.00
133B	Gneiss	68.49	0.04	19.74	0.57	0.01	0.04	0.48	4.21	4.66	0.11	1.68
135	Biotite graphite schist	50.52	0.62	28.67	8.93	0.02	0.28	0.02	0.63	5.51	0.10	4.70
136	Sandstone	90.50	0.09	6.826	0.48	0.01	0.03	0.02	0.10	1.61	0.05	0.28
142	Migmatitic Gneiss	68.99	0.09	18.82	0.98	0.02	0.18	0.29	3.55	5.66	0.37	1.05
143	Gneiss	62.49	0.30	23.02	2.12	0.02	0.29	0.39	1.84	6.50	0.60	2.41

Table 1 – (continuation)

Core	Lithotype	SiO <sub>2</sub>	TiO <sub>2</sub>	Al <sub>2</sub> O <sub>3</sub>	Fe <sub>2</sub> O <sub>3</sub>	MnO	MgO	CaO	Na <sub>2</sub> O	K <sub>2</sub> O	P <sub>2</sub> O <sub>5</sub>	LOI
144	Fine Granite	62.14	0.70	21.69	2.74	0.02	0.62	0.31	2.60	6.69	0.24	2.25
145	Altered Biotite schist	51.43	1.08	27.03	6.25	0.03	1.307	0.01	0.34	7.83	0.09	4.60
146	Biotite gneiss	66.86	0.40	18.86	1.98	0.02	0.44	0.76	2.88	6.30	0.51	1.00
147	Gneiss	67.44	0.32	19.13	1.96	0.03	0.33	0.36	3.01	6.41	0.37	0.63
148	Migmatitic Gneiss	65.85	0.24	20.59	2.09	0.02	0.28	0.63	3.23	5.83	0.38	0.86
162	Altered Biotite schist	50.37	1.17	26.29	10.32	0.04	2.06	0.01	0.10	8.27	0.11	1.26
164	Altered Biotite schist	46.82	1.10	30.41	13.23	0.21	0.89	0.01	0.40	5.60	0.25	1.06
165	Very altered Schist	48.69	1.19	30.45	8.74	0.03	1.58	0.02	0.60	7.72	0.09	0.88
166	Migmatitic Gneiss	68.21	0.03	21.35	1.27	0.01	0.07	0.52	3.22	3.89	0.04	1.38
167	Altered Schist	49.90	1.00	25.88	9.68	0.05	2.33	0.07	0.11	5.63	0.08	5.27
168	Gneiss	66.51	0.26	19.92	2.60	0.04	0.70	0.91	2.49	4.57	0.18	1.84
169A	Graphite schist	40.72	0.96	32.30	9.84	0.05	0.52	0.03	0.27	7.69	0.07	7.55
169B	Graphite schist	43.82	1.30	29.59	10.94	0.02	0.66	0.01	0.24	6.17	0.07	7.18
170	Altered schist	60.16	0.76	22.75	6.76	0.03	0.72	0.04	0.23	5.60	0.14	2.81
171	Biotite altered schist	37.83	1.91	23.04	17.00	0.06	5.63	0.02	0.04	7.27	0.05	7.14
172	Altered schist, red	50.15	1.06	25.95	9.95	0.04	1.66	0.02	0.20	6.19	0.11	4.65
173	Altered schist, red	50.10	0.80	28.15	9.87	0.08	0.40	0.01	0.57	5.29	0.14	4.57
174	Schist in contact with quartzite	65.71	0.23	22.81	1.60	0.01	0.91	0.02	0.27	6.69	0.02	1.72
175	Granada gneiss altered	65.28	0.23	21.66	2.17	0.02	0.58	1.48	4.13	2.94	0.12	1.41
176	Sandstone	81.53	0.15	12.86	0.65	0.005	0.35	0.03	0.20	3.46	0.11	0.67
177	Altered schist	49.21	1.10	27.47	7.89	0.03	0.80	0.02	0.14	6.92	0.13	6.30
178	Altered schist	42.54	0.96	30.39	9.13	0.02	1.82	0.01	0.21	7.31	0.12	7.55
179	Altered schist	51.58	0.83	24.07	8.51	0.03	2.84	0.02	0.24	7.02	0.17	4.67
180	Altered schist	43.14	0.55	27.45	8.22	0.05	0.59	0.04	0.38	5.12	0.10	14.36
181	Schist	45.55	1.31	27.02	11.01	0.03	1.66	0.01	0.09	8.28	0.05	4.98
182	Biotite gneiss	63.34	0.56	20.10	3.88	0.03	0.99	0.69	3.74	4.76	0.37	1.52
183	Altered schist	42.02	1.22	29.08	11.28	0.05	1.75	0.02	0.22	8.71	0.05	5.53
184	Granite coarse	69.53	0.17	18.07	1.61	0.02	0.58	0.23	4.63	3.75	0.07	1.33
185	Very altered Schist, red	38.09	0.62	25.02	11.80	0.04	0.37	0.01	0.21	4.87	0.08	18.89
186	Biotite gneiss fine	65.31	0.49	18.96	3.79	0.04	1.57	0.68	3.44	4.19	0.26	1.26
188	Very altered Schist	47.85	0.87	28.68	8.76	0.02	0.65	0.01	0.17	7.02	0.08	5.88
189	Very altered Gneiss	69.38	0.08	18.87	0.96	0.02	0.004	0.33	3.96	5.03	0.17	1.20
190A	Graphite schist	44.76	1.35	25.49	13.22	0.04	1.65	0.02	2.55	6.51	0.09	6.624
190B	Core of graphite level	44.53	0.82	27.87	4.76	0.005	0.67	0.01	0.40	6.65	0.05	14.23
192	Altered schist with quartzite vein	47.54	1.11	26.21	9.29	0.04	1.65	0.01	0.11	7.22	0.12	6.67
195	Gneiss	64.99	0.64	18.37	5.06	0.07	1.68	1.85	2.85	3.37	0.14	0.97
200	Biotite gneiss	63.10	0.72	20.00	3.54	0.02	1.33	2.14	4.80	2.81	0.22	1.29
201	Kyanite muscovite schist	55.31	0.92	23.03	6.96	0.12	2.32	0.98	1.58	4.49	0.07	4.22
202	Gneiss	59.85	0.59	22.15	3.02	0.03	1.01	0.57	1.65	8.27	0.67	2.17
205	Gneiss	69.35	0.21	17.09	1.49	0.03	0.63	1.51	4.80	3.83	0.17	0.89
208	Tourmalinite	50.11	3.67	12.71	18.68	0.08	2.68	3.13	1.67	4.65	2.03	0.58
209	Mylonitic Gneiss	54.26	0.82	21.92	7.35	0.06	2.01	1.04	0.51	8.33	0.28	3.41
210	Tourmalinite	44.20	2.05	17.23	16.30	0.14	7.88	1.36	1.44	6.93	0.66	1.81
211	Gneiss	64.55	0.10	21.76	1.14	0.01	0.77	1.85	5.54	2.99	0.41	0.88
215	Muscovite sericite schist	51.79	0.75	23.68	7.67	0.08	3.20	0.34	0.46	8.73	0.14	3.16

Table 1 – (continuation)

Core	Lithotype	SiO <sub>2</sub>	TiO <sub>2</sub>	Al <sub>2</sub> O <sub>3</sub>	Fe <sub>2</sub> O <sub>3</sub>	MnO	MgO	CaO	Na <sub>2</sub> O	K <sub>2</sub> O	P <sub>2</sub> O <sub>5</sub>	LOI
216	Gneiss	61.45	0.48	18.91	4.17	0.07	1.87	1.00	3.18	5.06	0.23	3.58
222	Gneiss fine	59.34	0.55	23.19	2.61	0.02	0.72	0.65	2.48	6.66	1.03	2.74
223	Granite	64.59	0.52	18.25	3.79	0.06	1.67	3.04	4.24	2.68	0.16	0.99
224	Migmatitic Gneiss, porphyric feldspar	49.93	0.79	30.91	1.82	0.01	1.42	0.03	0.40	10.13	0.06	4.52
226	Schist	46.49	0.80	30.78	3.02	0.02	1.61	0.54	0.21	11.76	0.52	4.26
227	Fresh Biotite muscovite schist	51.81	0.85	25.72	5.63	0.06	2.03	0.21	0.57	9.55	0.27	3.33
228	Migmatitic Gneiss	48.96	0.62	15.98	11.45	0.19	7.16	11.41	2.26	0.85	0.26	0.86
229	Gneiss	63.07	0.24	22.05	1.92	0.02	0.69	0.45	2.83	6.33	0.27	2.12
231	Migmatitic Gneiss	66.92	0.22	18.90	1.62	0.03	0.64	0.48	2.79	6.35	0.35	1.71
232	Altered Biotite muscovite schist	49.02	0.93	28.12	5.67	0.02	1.98	0.01	0.18	9.43	0.24	4.39
233	Gneiss	65.27	0.40	19.18	2.28	0.02	0.57	0.62	2.99	6.38	0.68	1.61
235	Gneiss	52.70	0.08	29.40	1.73	0.02	1.61	0.003	0.16	10.38	0.10	3.83
236	Gneiss fine	56.10	0.06	27.00	1.61	0.01	1.67	0.03	0.20	9.67	0.03	3.62
242	Biotite muscovite schist	43.71	1.08	28.60	6.64	0.04	2.33	2.65	0.18	10.40	2.87	1.49
243	Biotite gneiss	55.55	0.24	25.36	3.11	0.02	1.65	0.28	0.16	9.40	0.53	3.69
244	Biotite muscovite gneiss	50.25	0.56	30.91	3.85	0.02	1.71	0.08	0.65	8.98	0.16	2.82
245	Muscovite schist	56.47	0.19	26.79	2.50	0.005	0.54	0.01	0.25	10.22	0.15	2.86
247	Muscovite quartz schist	52.45	1.06	29.11	2.03	0.01	1.57	0.01	0.18	9.83	0.05	3.73
248	Biotite gneiss	67.84	0.42	17.02	2.96	0.03	1.47	1.52	3.05	4.08	0.29	1.32
249	Biotite gneiss	75.29	0.44	14.95	1.29	0.01	1.20	0.04	0.14	5.17	0.14	1.33
251	Biotite gneiss	61.46	0.61	20.75	5.39	0.10	1.67	0.84	2.49	3.93	0.26	2.49
254	Fine Gneiss	67.01	0.20	19.05	1.53	0.02	0.48	0.54	4.32	4.87	0.45	1.52
255	Gneiss	64.47	0.35	21.64	2.45	0.03	0.69	1.00	4.43	3.09	0.28	1.58
256	Gneiss	61.36	0.26	21.24	2.41	0.02	0.80	1.65	2.56	6.08	1.19	2.41
261	Altered schist, red	52.56	0.97	28.08	6.88	0.03	2.24	0.01	0.17	7.99	0.08	0.99
262	Very altered Schist	48.72	0.40	27.78	14.47	0.03	0.74	0.04	0.35	5.79	0.34	1.35
263	Gneiss	64.08	0.45	20.80	2.86	0.04	0.95	0.34	3.31	5.87	0.41	0.89
264	Muscovite schist	53.25	0.63	28.63	3.60	0.03	2.39	0.02	0.15	9.66	0.12	1.54
265	Very altered Schist	47.84	1.01	28.79	10.02	0.09	1.95	0.02	0.24	8.77	0.11	1.16
266	Gneiss	67.60	0.29	17.54	1.95	0.02	0.43	0.64	4.19	5.24	1.02	1.10
267	Altered schist	42.54	1.04	30.82	13.04	0.07	2.78	0.03	0.27	7.59	0.17	1.65
270	Gneiss Migmatitic	65.93	0.11	20.46	1.39	0.03	0.62	0.57	4.24	5.23	0.18	1.24
271	Muscovite quartz schist	59.51	0.27	25.82	1.89	0.01	0.86	0.05	0.28	9.62	0.06	1.68
272	Gneiss	60.06	0.83	21.16	3.74	0.02	0.94	0.84	2.10	7.01	1.56	1.76
Basal Complex												
84A	Altered Biotite schist	44.64	1.20	28.83	10.33	0.02	0.74	0.01	0.26	6.36	1.23	6.38
84B	Altered schist	58.17	0.42	25.94	3.72	0.02	0.43	0.01	0.48	7.14	0.05	3.62
85	Altered Gneiss	67.91	0.20	19.28	1.48	0.02	0.45	2.62	5.70	1.08	0.44	0.80
86	Altered Biotite gneiss	68.27	0.19	19.44	1.45	0.02	0.50	2.34	5.69	1.13	0.03	0.94
87	Biotite gneiss	69.58	0.18	17.93	1.63	0.03	0.50	2.02	5.82	1.83	0.04	0.43
88	Altered schist	42.73	1.05	29.31	13.60	0.03	0.34	0.02	0.25	6.04	0.16	6.47
130	Gneiss	68.51	0.31	18.02	1.50	0.01	0.29	0.40	2.95	6.83	0.37	0.81
131	Granite gneissic	68.81	0.30	17.66	1.73	0.02	0.31	0.58	3.13	6.33	0.37	0.77
134	Gneiss	67.05	0.13	19.41	1.27	0.03	0.50	0.52	3.27	6.02	0.24	1.56
137	Gneiss in waterfalls	49.75	0.64	29.02	7.92	0.07	1.13	0.01	0.04	6.36	0.11	4.93

Table 1 – (continuation)

Core	Lithotype	SiO <sub>2</sub>	TiO <sub>2</sub>	Al <sub>2</sub> O <sub>3</sub>	Fe <sub>2</sub> O <sub>3</sub>	MnO	MgO	CaO	Na <sub>2</sub> O	K <sub>2</sub> O	P <sub>2</sub> O <sub>5</sub>	LOI
138	Leucogranite with quartz vein	65.95	0.32	19.74	2.06	0.02	1.02	0.47	2.77	6.35	0.19	1.09
139	Granite	65.31	0.22	20.22	1.82	0.03	0.56	1.17	5.40	4.38	0.14	0.74
161	Granite in blocks	55.69	1.05	26.17	9.14	0.02	0.61	0.01	0.17	6.40	0.06	0.67
163	Granite	69.69	0.17	17.97	1.32	0.02	0.63	1.19	6.48	1.38	0.11	1.04
191	Granite	65.50	0.21	21.61	1.09	0.01	0.27	0.73	5.80	3.01	0.21	1.56
193	Granite	68.76	0.32	17.47	2.52	0.03	1.08	2.71	5.01	1.47	0.08	0.55
194	Granite	64.20	0.35	21.54	2.75	0.02	0.90	1.94	3.80	2.23	0.13	2.13
196	Granite	67.53	0.21	18.62	1.70	0.04	1.21	3.67	5.23	0.99	0.10	0.70
197	Granite	70.07	0.15	16.46	1.34	0.03	1.00	3.08	6.35	0.74	0.15	0.61
198	Granite	65.35	0.36	18.46	3.01	0.04	0.86	0.81	3.67	4.96	0.82	1.67
199	Granite	58.84	0.83	21.91	2.80	0.09	0.98	1.01	2.45	7.46	1.15	2.48
212	Biotite gneiss	61.54	0.42	22.07	2.82	0.05	1.46	0.94	3.02	5.30	0.17	2.21
213	Granite gneissic	62.25	0.20	22.18	1.10	0.03	0.45	0.41	4.23	6.80	0.33	2.03
214	Gneiss mylonitic	53.24	0.77	23.56	7.17	0.07	2.60	0.45	0.87	8.16	0.14	2.95
219	Schist brown (fresh)	50.87	0.94	25.00	7.92	0.04	1.88	0.03	0.13	9.31	0.23	3.65
220	Biotite gneiss	53.69	0.47	24.10	3.84	0.08	0.85	6.98	6.48	0.17	0.15	3.96
221	Granite grey	62.59	0.47	18.02	4.08	0.06	2.08	2.39	5.06	2.45	0.12	2.69
225	Granite	65.59	0.43	19.19	2.61	0.04	0.80	0.70	3.64	5.57	0.17	1.26
230	Gneissic Granite	63.70	0.24	20.79	1.73	0.02	0.57	0.52	3.78	6.37	0.42	1.84
237	Fine banded Granite	66.70	0.31	18.47	1.76	0.04	1.12	2.85	6.26	1.56	0.20	0.72
238	Migmatitic Gneiss	60.19	1.11	18.69	5.33	0.09	1.50	3.09	3.71	4.64	0.56	1.09
239	Biotite gneiss	60.05	1.17	19.86	3.57	0.04	1.43	1.53	2.23	7.42	0.98	1.73
246	Biotite gneiss	66.21	0.43	18.63	3.28	0.04	1.22	1.98	5.13	1.57	0.10	1.40
250	Gneiss	65.16	0.25	19.62	2.54	0.05	1.01	2.16	5.73	2.01	0.14	1.34
252	Gneiss	64.00	0.38	20.25	2.07	0.02	0.81	0.59	3.15	6.31	0.47	1.94
253	Gneiss	70.43	0.30	15.81	2.27	0.04	0.99	2.09	5.69	1.56	0.16	0.65
259	Gneiss	66.91	0.37	15.86	3.48	0.07	1.76	2.20	5.11	1.72	0.08	2.44
260	Gneiss	66.90	0.36	16.62	3.51	0.05	1.58	1.70	6.18	1.92	0.11	1.08

In the gneisses of the Lower Member ( $n = 93$ ), there are significant correlations between the oxides from Fe<sub>2</sub>O<sub>3</sub> and MgO ( $r = 0,85$ ), Fe<sub>2</sub>O<sub>3</sub> and MnO ( $r = 0,83$ ), MnO and MgO ( $r = 0,80$ ), Fe<sub>2</sub>O<sub>3</sub> and TiO<sub>2</sub> ( $r = 0,78$ ), and SiO<sub>2</sub> and Al<sub>2</sub>O<sub>3</sub> ( $r = -0,78$ ) (Fig. 4); while for the fresh schists of the Lower Member ( $n = 26$ ) significant correlations were observed between CaO and Na<sub>2</sub>O ( $r = 0,81$ ), SiO<sub>2</sub> and Al<sub>2</sub>O<sub>3</sub> ( $r = -0,81$ ), MnO and CaO ( $r = 0,80$ ) and Fe<sub>2</sub>O<sub>3</sub> and TiO<sub>2</sub> (Fig. 5). On the other hand, for the altered schists of this formation ( $n = 63$ ), no significant correlation was observed among the analyzed oxides. When considering only the schists of the Upper Member ( $n = 20$ ), significant correlations were observed between Na<sub>2</sub>O and CaO ( $r = 0,95$ ), SiO<sub>2</sub> and Al<sub>2</sub>O<sub>3</sub> ( $r = -0,82$ ) and TiO<sub>2</sub> and MgO ( $r = 0,72$ ) (Fig. 6).

Radiometric data of the study site regarding <sup>40</sup>K were presented by Duarte & Bonotto (2006), which seem to be corre-

lated with the levels of K<sub>2</sub>O shown in Table 1 for the gneisses and gneissic granite cores of the Basal Complex ( $n = 34$ ), as seen in Figure 7, thus showing the reading compatibility of the two spectrometric methods used. This compatibility was also observed for the schist samples from the Upper Member ( $n = 20$ ;  $r = 0,77$ ) (Fig. 7).

Susceptibility to weathering of many rock forming minerals can be determined directly by observing the abundance of primary minerals in the saprolite formed at different stages of weathering of a particular rock type. Al<sub>2</sub>O<sub>3</sub> concentration has been widely used for this evaluation, since Al<sup>3+</sup> is a relatively immobile ion during chemical weathering and, while other oxides are lost during the weathering process, the relative concentration of Al<sub>2</sub>O<sub>3</sub> increases during the weathering process (Faure, 1991). This can be seen in samples of gneisses and fresh schists of the Ticunzal Forma-

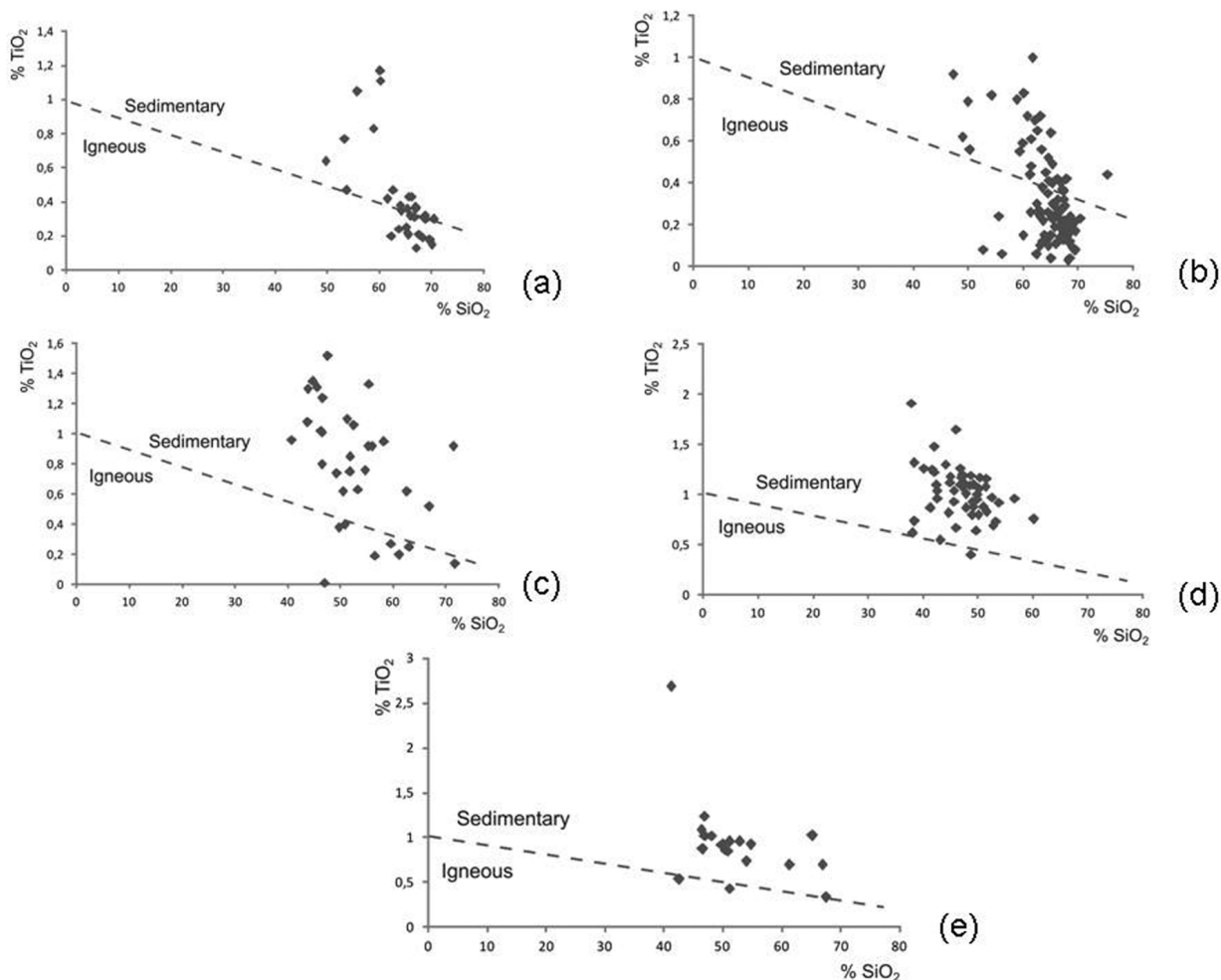


**Figure 3** – Diagram  $\text{TiO}_2$ - $\text{SiO}_2$  (Tarney, 1976) for the (a) gneiss and gneissic granites of the Basal Complex, (b) gneiss of the Lower Member, Ticunzal Formation, (c) fresh schists of the Lower Member, Ticunzal Formation and (d) altered schists of the Lower Member, Ticunzal Formation and (e) schists of the Upper Member, Ticunzal Formation.

tion, since the correlations between  $\text{Al}_2\text{O}_3$  and  $\text{SiO}_2$  are significant and inverse. The same occurs with other correlations, for example, between  $\text{Fe}_2\text{O}_3$  and  $\text{TiO}_2$ , indicating that these oxides were accumulating during weathering, thus affecting the gneisses and fresh schists of the Ticunzal Formation.

The evaluation of the organic matter importance for the binding of uranium and thorium was initially performed by applying correlation statistical tests to the results of LOI (loss on ignition), uranium (eU) and thorium (eTh) in all samples (eU and eTh data described by Duarte & Bonotto, 2006). For the gneisses of the Lower Member, the following correlations were determined:  $r = 0,11$  (eU and LOI) and  $r = 0,06$  (eTh and LOI). For the fresh schists of the Lower Member, the following correlations were found:  $r = -0,01$  (eU and LOI) and  $r = 0,39$  (eTh and LOI). While for the altered schists of this formation, the following correlations were

obtained:  $r = -0,11$  (eU and LOI) and  $r = -0,10$  (eTh and LOI). When considering only the Upper Member schists, the following correlations were found:  $r = -0,22$  (eU and LOI) and  $r = 0,08$  (eTh and LOI). The correlation values were non-significant for all cases, thus suggesting that the organic matter (LOI) does influence the absorption of the radioelements U and Th.

For a more detailed evaluation, Table 2 shows the correlation coefficients among organic matter, uranium (eU) and thorium (eTh) levels obtained for the samples that underwent colorimetric analysis (Hach, 1992). The determined values also confirm that organic matter does not influence uranium and thorium binding, since high concentrations of these radioelements were found where organic matter is virtually absent, while samples with high levels of graphite did not have high levels of U and Th. The highest U concentration of 467 ppm was determined

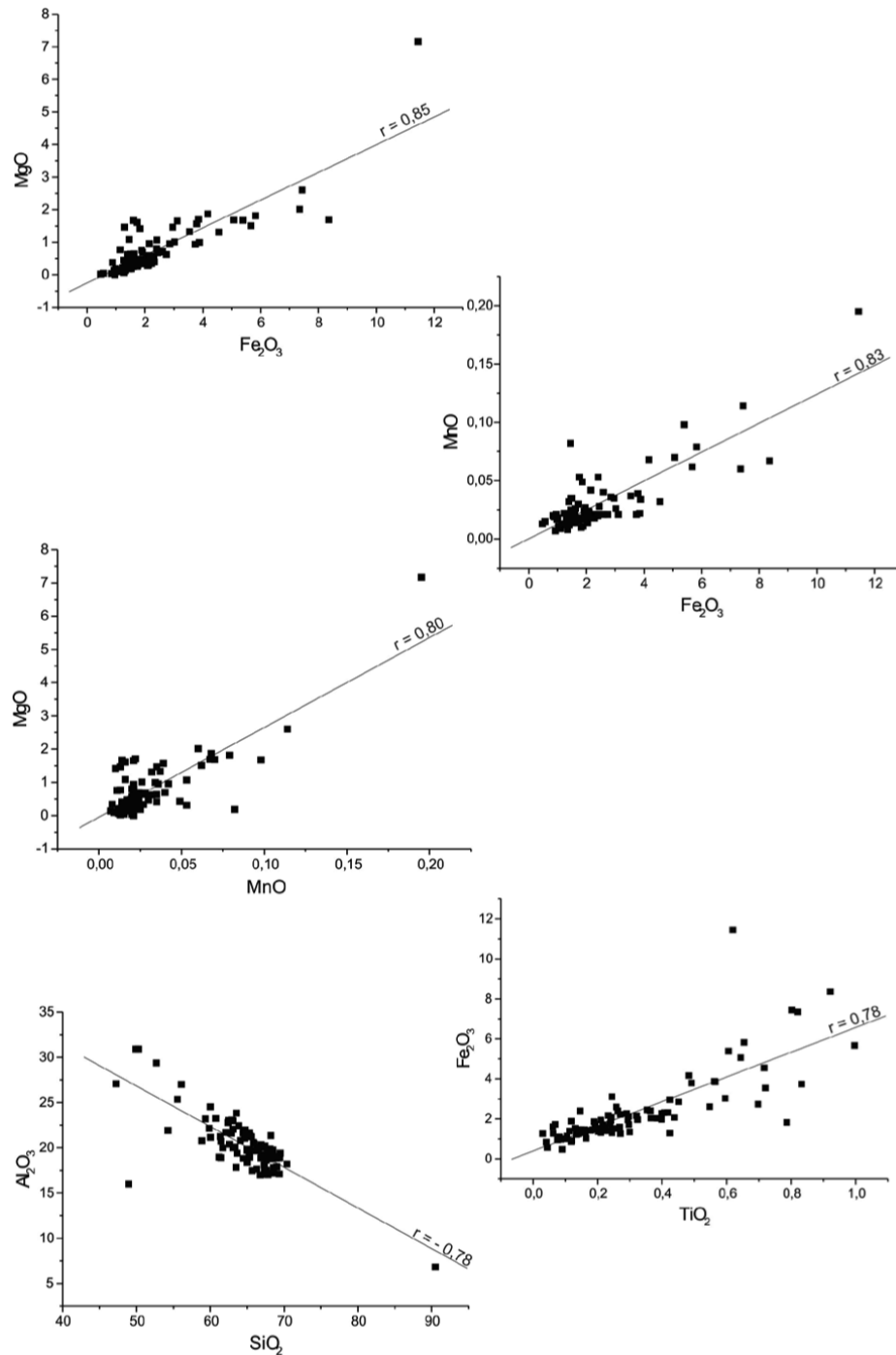


**Figure 4** – Correlations for the analyzed oxides of gneiss samples from the Lower Mb., Ticunzal Fm. (n = 93).

for sample 227 of the Lower Member, Ticunzal Fm. (biotite muscovite schist), sampled in the NW portion of the area. The mineralogical analysis of this sample indicated the presence of apatite, a mineral commonly recognized as having high concentrations of this element.

Table 3 shows the results obtained for uranium concentration and  $^{234}\text{U}/^{238}\text{U}$  activity ratio by alpha spectrometry analysis of selected samples of schists and gneisses of the Lower Member of the Ticunzal Formation, as well as the values of uranium concentration ( $\text{eU} = ^{226}\text{Ra}$ ) determined by gamma-ray spectrom-

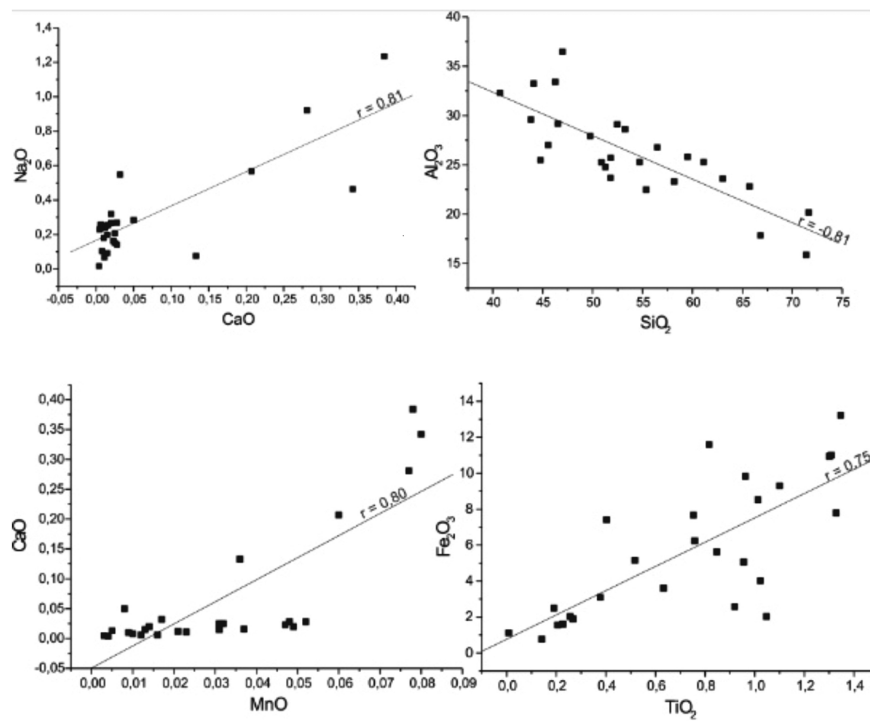


Figure 5 – Correlation for the analyzed oxides of fresh schist samples from the Lower Mb., Ticznal Fm. (n = 26).

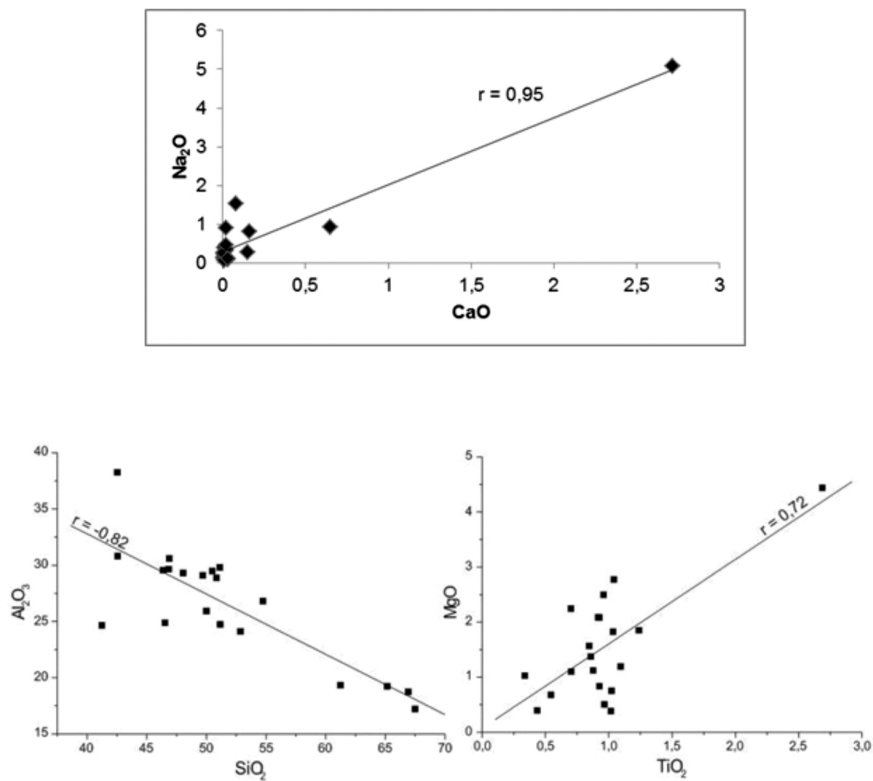
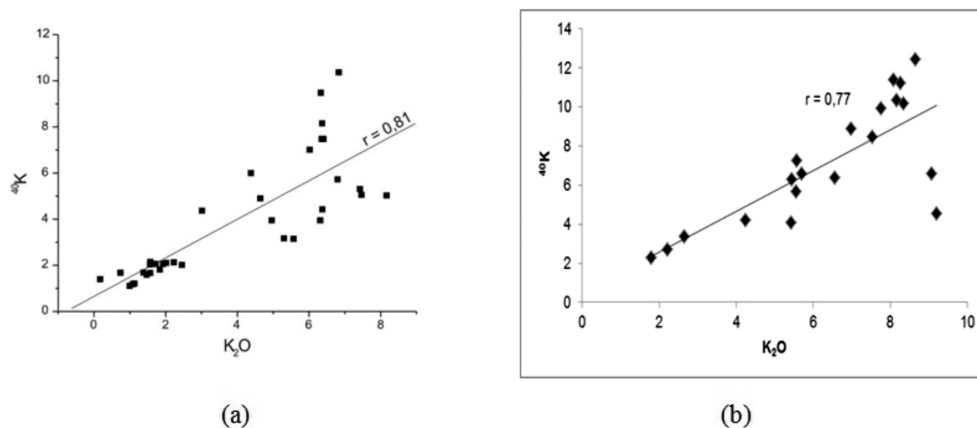


Figure 6 – Correlation for the analyzed oxides of the schist samples from the Upper Mb., Ticznal Fm. (n = 20).





**Figure 7** – Correlation between  $K_2O$  and  $^{40}K$  for the samples from (a) gneiss and gneissic granites from the Basal Complex ( $n = 34$ ) and (b) schists from the Upper Mb., Ticunzal Fm. ( $n = 20$ ).

**Table 2** – Correlation between organic matter, uranium (eU) and thorium (eTh) for selected samples of the study area.

Core sample	Lithostratigraphic unit and sampled lithotype	eU (ppm) <sup>1</sup>	eTh (ppm) <sup>1</sup>	Organic Matter (OM) (%)
55B	Lower Member, Ticunzal Formation – Sand with heavy sediments	4.98	29.63	2.46
98	Arraias Formation – Graphite schist	3.47	13.50	1.62
101	Upper Member, Ticunzal Formation – Graphite schist	0.93	17.92	2.36
106	Lower Member, Ticunzal Formation – Graphite schist	13.65	13.06	1.68
116	Lower Member, Ticunzal Formation – Graphite schist	6.78	8.68	3.64
152	Upper Member, Ticunzal Formation – Graphite schist	8.50	24.72	5.42
190B	Lower Member, Ticunzal Formation – Graphite schist	4.51	16.29	3.52
227	Lower Member, Ticunzal Formation – Biotite muscovite schist	467.24	36.30	1.64
242	Lower Member, Ticunzal Formation – Biotite muscovite schist	182.39	254.06	0.49
272	Lower Member, Ticunzal Formation – Gneiss	12.34	233.30	0.69
Correlation coefficient (OM)		$r = -0.15$	$r = -0.33$	

<sup>1</sup>Analytical uncertainty  $\pm 10\%$  corresponding to a standard deviation of  $1\sigma$ . Data presented by Duarte & Bonotto (2006).

etry with NaI(Tl) scintillation detector (Duarte & Bonotto, 2006).  $^{234}U/^{238}U$  activity ratios equal to one, within the analytical uncertainties, were found for 19 samples, indicating radioactive equilibrium between  $^{234}U$  and  $^{238}U$  during the last million years and suggesting that there was no mobilization of these isotopes on this timescale or if there was, both were equally affected.

The eU/U ratios were determined for the Lower Member samples, with eU given by spectrometric reading and U by alpha spectrometry (Table 3). The uncertainty calculation was based on the theorem of error propagation, assuming that there is no error on time reading (Lyons, 1991). The samples 24, 26B, 36A, 60, 68, 119, 132, 142, 147 and 164 have eU/U value close to one,

**Table 3** – Concentration of U (ppm),  $^{234}\text{U}/^{238}\text{U}$  activity ratio, eU (ppm) and eU/U ratio for selected samples from the Lower Member, Ticunzal Formation. All analytical uncertainties correspond to standard deviation of  $1\sigma$ .

Sample	Sampled lithotype	U (ppm)	A.R. $^{234}\text{U}/^{238}\text{U}$	eU (ppm) <sup>1</sup>	eU/U
11	Altered schist	18.54 ± 4.29	1.08 ± 0.19	14.32 ± 1.05	0.77 ± 0.11
19	Altered schist	30.89 ± 4.23	1.01 ± 0.09	17.96 ± 1.02	0.58 ± 0.04
24	Mica schist	33.53 ± 14.21	0.93 ± 0.22	38.49 ± 1.02	1.15 ± 0.19
26B	Altered schist	22.57 ± 4.83	1.18 ± 0.17	20.17 ± 1.04	0.89 ± 0.10
36A	Lateritic Canga	14.29 ± 5.36	1.04 ± 0.34	18.44 ± 1.02	1.29 ± 0.38
37	Biotite altered schist	33.83 ± 14.91	1.15 ± 0.24	19.03 ± 1.03	0.56 ± 0.09
60	Fine grey Gneiss	44.71 ± 5.78	1.15 ± 0.08	45.74 ± 1.01	1.02 ± 0.05
68	Altered schist	9.07 ± 1.59	0.87 ± 0.14	11.91 ± 1.05	1.31 ± 0.18
90	Gneiss	24.38 ± 7.40	1.08 ± 0.24	16.83 ± 1.02	0.69 ± 0.11
91	Gneiss	10.91 ± 2.99	1.05 ± 0.27	9.01 ± 1.05	0.83 ± 0.16
106	Graphite schist	38.98 ± 11.16	0.91 ± 0.15	19.10 ± 1.02	0.49 ± 0.06
116	Graphite schist	73.59 ± 17.74	0.95 ± 0.11	23.44 ± 1.02	0.32 ± 0.03
119	Altered schist	18.25 ± 5.36	1.24 ± 0.25	18.85 ± 1.02	1.03 ± 0.18
123	Gneiss Migmatitic	71.63 ± 28.06	0.98 ± 0.16	21.66 ± 1.01	0.30 ± 0.04
132	Biotite altered schist	27.49 ± 6.17	0.89 ± 0.14	36.44 ± 1.01	1.33 ± 0.18
142	Gneiss Migmatitic	3.69 ± 0.61	1.03 ± 0.19	3.35 ± 1.15	0.91 ± 0.13
147	Gneiss	22.91 ± 14.96	0.93 ± 0.40	21.09 ± 1.02	0.92 ± 0.28
164	Biotite altered schist	11.63 ± 4.64	1.05 ± 0.38	15.27 ± 1.04	1.31 ± 0.36
190B	Graphite schist	38.61 ± 7.98	1.15 ± 0.15	4.91 ± 1.14	0.13 ± 0.01

<sup>1</sup>Data presented by Duarte & Bonotto (2006).

indicating radioactive equilibrium in the uranium decay series until  $^{226}\text{Ra}$ . The other samples show values of eU/U lower than one, thus indicating the preferential mobilization of  $^{226}\text{Ra}$  in the uranium decay chain, possibly due to the weathering processes of the region.

## CONCLUSION

This work contributed to better understanding of the issues related to the occurrence of the natural radioelements U, Th and  $^{40}\text{K}$  in the area of the Rio Preto Project (GO), thanks to the integration of petrographic and geochemical analysis results. The petrographic analysis suggest and confirm the high degree of rock alteration in the region, which was also confirmed by significant and inverse correlations between  $\text{Al}_2\text{O}_3$  and  $\text{SiO}_2$ , since  $\text{Al}^{3+}$  is a relatively immobile ion during chemical weathering, the relative concentration of  $\text{Al}_2\text{O}_3$  increases during the weathering processes. In addition, the eU/U ratio lower than one found for several samples also suggest preferential mobilization of  $^{226}\text{Ra}$  in the uranium decay series, possibly due to weathering processes of the region. The chemical analysis of the main oxides present in the rocks allowed us to find several significant correlations, for example, between  $\text{K}_2\text{O}$  and  $^{40}\text{K}$

for the schists of the Upper Member of the Ticunzal Formation and for the gneisses and gneissic granite of the Basal Complex, indicating the compatibility of the X-ray fluorescence and gamma-ray spectrometry reading methods. The results did not show any correlation between the presence of organic matter and the binding of uranium and thorium; however, the mineralogical analysis shows that the highest uranium concentration is correlated with apatite, a mineral known for the accumulation of this radioelement. Further studies are required to determine whether this occurrence is occasional or the result of geochemical processes.

## ACKNOWLEDGEMENTS

The authors thank CNPq for the scholarship (Process 14/2798-3) and FAPESP for the financial support given to the project (Process 99/12476-0).

## REFERENCES

ALMEIDA FFM de, HASUI Y & NEVES BBB. 1977. Províncias estruturais brasileiras. In: Simpósio de Geologia Nordeste, 8: Campina Grande. Anais... Campina Grande: SBG, p. 363–391.

- ANDRADE SM, SOUZA EL & OLIVEIRA AG. 1981. Projeto Rio Preto – Mapeamento Geológico – Escala 1:25.000. Relatório Técnico, Nuclebrás/SUPPM, Poços de Caldas.
- ANDRADE SM, LIBERAL GS & SANTOS FILHO JL. 1985. Depósitos de urânio de Campos Belos e Rio Preto – Goiás. In: SCHOBENHAUS FILHO C (Ed.). Principais Depósitos Minerais do Brasil. DNPM, Rio de Janeiro, v.1, p.169–175.
- BONOTTO DM. 2004. Radioatividade nas águas: da Inglaterra ao Guarani. Editora UNESP, São Paulo, 251 p.
- CAMPOS JEG, MONTEIRO CF & DARDENNE MA. 2009. Conglomerado São Miguel no Vale da Lua, sul da Chapada dos Veadeiros, GO – Cenário exótico de rara beleza modelado pela erosão fluvial. In: WINGE M, SCHOBENHAUS FILHO C, BERBERT-BORN M, QUEIROZ ET, CAMPOS DA, SOUZA CR & FERNANDES ACS (Eds.). Sítios Geológicos e Paleontológicos do Brasil. DNPM, Brasília, v. 2, 8 p.
- CHAPADA 2000. Available on: <<http://www.chapada.com/>>. Access on: 10 dez. 2000.
- DARDENNE MA. 2000. The Brasília Fold Belt. In: CORDANI UG, MILANI EJ & THOMAZ FILHO A (Eds.). Tectonic Evolution of South America. DNPM, Rio de Janeiro, p. 231–263.
- DUARTE CR & BONOTTO DM. 2000. A radioatividade na área do Projeto Rio Preto (GO). *Geochim. Brasil.*, 14 (2): 191–207.
- DUARTE CR & BONOTTO DM. 2006. Gamaespectrometria aplicada ao Projeto Rio Preto (GO). *Geochim. Brasil.*, 20 (3): 278–294.
- FAURE G. 1991. Principles and applications of inorganic geochemistry. Prentice Hall, Upper Saddle River, 626 p.
- FIGUEIREDO FILHO PM, OLIVEIRA AG & LIBERAL GS. 1982. Projeto Rio Preto. Relatório Técnico, Nuclebrás/SUPPM, Poços de Caldas.
- GOMES CB. 1984. Técnicas analíticas instrumentais aplicadas à Geologia. Edgard Blücher, São Paulo, 217 p.
- HACH 1992. Water analysis handbook. Hach Co., Loveland, 2nd edn., 831 p.
- IVANOVICH M & HARMON RS. 1992. Uranium Series Disequilibrium: Applications to Environmental Problems, 2<sup>nd</sup> edition. Oxford Univ. Press, Oxford, 571 p.
- JAVARONI JH & MACIEL AC. 1985. Prospecção e pesquisa de urânio no Brasil: atuação da Nuclebrás (1975-1984). In: SCHOBENHAUS FILHO C (Ed.). Principais Depósitos Minerais do Brasil. DNPM, Rio de Janeiro, v. 1, p. 81–87.
- LACERDA FILHO JV, REZENDE A & SILVA A. 2000. Geologia e recursos minerais do Estado de Goiás e do Distrito Federal. Escala 1:500.000. In: CPRM (Ed.) Programa de Levantamentos Geológicos Básicos do Brasil. CPRM/METAGO/UnB, Brasília, 184 p.
- LANGMUIR D. 1978. Uranium solution-mineral equilibria at low temperatures with applications to sedimentary ore deposits. *Geochim. Cosmochim. Acta*, 42: 547–569.
- LYONS L. 1991. A practical guide to data analysis for physical science students. Cambridge University Press, Cambridge, 95 p.
- MAJDALANI S. 1999. Crescem as reservas brasileiras de urânio. *Rev. Brasil Nuclear*, 18: 22.
- MARTINS FAL. 1999. Análise Faciológica e Estratigráfica do Paleoproterozóico: Sequência Araí do Parque Nacional da Chapada dos Veadeiros, Goiás. Dissertação (Mestrado em Geociências) – Programa de Pós-graduação em Geociências, Instituto de Geociências, Universidade de Brasília, 137 p.
- PINTO MN. 1986. Residuais de aplainamentos na Chapada dos Veadeiros – Goiás. *Revista Brasileira de Geografia*, 48 (2): 187–197.
- ROSS JLS. 1985. Relevo brasileiro: uma nova proposta de classificação. *Rev. Depto. Geog.*, 4: 25–39.
- TARNEY J. 1976. Geochemistry of Archean high-grade gneisses, with implications as to the origin and evolution of the Precambrian Crust. In: WIDLEY BF (Ed.). The early history of the earth. John Wiley, London, p. 405–417.

## NOTES ABOUT THE AUTHORS

**Cynthia Romariz Duarte.** Graduated in Geology at UNESP – Universidade Estadual Paulista (1994). M.Sc. (1997) and Ph.D. (2002) in Regional Geology also at UNESP – Universidade Estadual Paulista. Currently, teaches undergraduate and graduate courses at Universidade Federal do Ceará. Has experience in the field of Geosciences, with emphasis on Geoprocessing and its environmental applications. Participates in the Research Groups “Hydrochemistry and Radioactivity in Geosphere” and “Radon net at Rio Grande do Norte (RnRN)”.

**Daniel Marcos Bonotto.** Graduated in Physics at UNESP – Universidade Estadual Paulista (1978); M.Sc. (1986) and Ph.D. in Geophysics at USP – Universidade de São Paulo (1986). Currently, is a full Professor of Geochemistry at UNESP – Universidade Estadual Paulista. Has experience in the field of Geosciences, with emphasis on Nuclear Geophysics and Isotope Geochemistry, working in the following areas: natural radioactivity, hydrochemical analysis, surface waters and groundwater. Since 1988 coordinates the research group “Hydrochemistry and Radioactivity in Geosphere”.

**Marcos Aurélio Farias de Oliveira.** Graduated in Geology at USP – Universidade de São Paulo (1966); M.Sc. (1969) and Ph.D. (1972) in Geosciences, both at USP – Universidade de São Paulo. Currently, is a retired Professor from UNESP – Universidade Estadual Paulista, performing teaching and researching activities as a Volunteer Professor. Has experience in the field of Geosciences, with emphasis on Metamorphic Petrology and Regional Geology, working mainly on the following topics: petrology, granulite, charnockite-granite association, geochemistry, isotope geology and geological mapping. Coordinates the research group “Evolution of Metamorphic Terrains” and is currently the Chief Editor of the periodical “Geociências” of UNESP.